photonics

MDPI

Article

Research on VMD-Based Adaptive TDLAS Signal Denoising Method

Minghui Mao [1,2], Jun Chang [1,*], Jiachen Sun [1], Shan Lin [1,2] and Zihan Wang [1]

[1] Shandong Provincial Key Laboratory of Laser Technology and Application, School of Information Science and Engineering, Shandong University, Qingdao 266200, China
[2] Key Laboratory of Laser and Infrared System of Ministry of Education, Shandong University, Qingdao 266200, China
* Correspondence: changjun@sdu.edu.cn

Abstract: We propose an adaptive algorithm that is a Variational Mode Decomposition (VMD) optimized by the particle swarm optimization (PSO) algorithm, named PSO-VMD. The method selects the envelope entropy of the last intrinsic mode function (IMF) in the VMD as the fitness function of the PSO and 1/10 of the maximum value of the correlation coefficient between the IMFs and the standard signal as the threshold of the correlation coefficient. In the processing of simulated and experimental second harmonic signals, a series of standards, including the same correlation coefficient threshold and standard signal, are used to adaptively achieve noise reduction processing. After processing a simulated signal using PSO-VMD, the signal-to-noise ratio (SNR) was improved by 4.03877 dB and the correlation coefficient (R^2) between the gas concentration and the second harmonic maximum was improved from 0.97743 to 0.99782. In the processing of an experimental signal, the correlation coefficient (R^2) was 0.99733. The mean value and standard deviation of the second harmonic signal of multiple cycles processed by PSO-VMD were improved compared to the unprocessed experimental signal. This demonstrated that the method has the advantage of being reliable and stable.

Keywords: TDLAS; VMD; PSO; adaptive

Citation: Mao, M.; Chang, J.; Sun, J.; Lin, S.; Wang, Z. Research on VMD-Based Adaptive TDLAS Signal Denoising Method. *Photonics* **2023**, *10*, 674. https://doi.org/10.3390/photonics10060674

Received: 10 May 2023
Revised: 7 June 2023
Accepted: 8 June 2023
Published: 11 June 2023

1. Introduction

Tunable diode laser absorption spectroscopy (TDLAS) is widely used in gas detection because of its high sensitivity, high accuracy, and rapid response time [1–3]. However, during the detection process of TDLAS, it is unavoidably affected by environmental, optical, and electronic noise, as well as other types of noise, thereby affecting the detection sensitivity and the signal-to-noise ratio (SNR) of the signal of the TDLAS system. There are two general ways to improve the sensitivity and SNR of a signal in a TDLAS system: one is to enhance the signal, and the other is to reduce the noise [4]. However, the methods of signal enhancement usually change the system's structure, which leads to an increase in cost [5]. The way to reduce noise in TDLAS systems usually uses software filtering [6,7], which only needs partial computational resources and does not require additional electronic and optical devices [8–11].

At present, Savitzky–Golay (SG) filtering is a common method for signal time domain analysis and is usually combined with the minimum-squares method [12] for signal processing, but SG filtering usually depends on a given window size and polynomial fitting steps. The wavelet transform is non-adaptive in processing different signals and needs to choose different wavelet basis functions, decomposition layers, and thresholds depending on the signal [13]. Compared with the SG filter and wavelet transform, Empirical Mode Decomposition (EMD) does not need to select the basis function and is an adaptive signal processing method [14], but the EMD method has the phenomena of modal aliasing and the endpoint effect. The Ensemble Empirical Mode Decomposition (EEMD) method can eliminate the

phenomena of modal aliasing and the endpoint effect in EMD by adding different white noise to the signal based on EMD [15], but white noise is mixed into the signal, resulting in a poor noise reduction effect. In addition, Variational Mode Decomposition (VMD) converts the decomposition process of the signal into the framework of the variational problem, which decomposes the signal into a series of intrinsic mode functions with different center frequencies with finite bandwidth [16], thus effectively solving the corresponding modal mixing, endpoint effect, and mixing white noise phenomena in EMD and EEMD. However, the K and α parameters in VMD significantly affect the decomposition results, and they are usually set up based on empirical values or an artificial search for the optimal K and α parameter values, which requires a lot of time and ignores the influence between the two parameters.

Therefore, in order to find the optimal values of K and α more precisely and quickly, this paper provides a method to optimize K and α using the particle swarm optimization algorithm (PSO). The envelope entropy value of the last intrinsic mode function (IMF) component after VMD processing is used as the fitness function in the PSO algorithm. The particles are continuously searched until the minimum value of the fitness function in the solution space is found, along with the corresponding values of K and α, which are the optimal solutions in that space. Then, the correlation coefficients between each of the IMF components and the given standard sample are calculated and compared with the magnitudes of the given correlation coefficient thresholds to determine the IMFs needed for the last reorganization of the signal and eventually complete the signal noise reduction process. In a simulated signal noise reduction process, compared with the SG filter and wavelet transform, our algorithm had the best results in terms of SNR and linearity. In the noise reduction processing of an experimental signal, the same standard signal, correlation coefficient threshold, and series of conditions were used as for the simulated signal, and a good noise reduction effect in terms of stability and linearity was obtained, proving that the PSO-VMD algorithm is an effective adaptive noise reduction method.

2. Wavelength Modulation Spectroscopy

The laser output's optical frequency and optical power after the scanning signal and modulation signal are injected into the laser can be expressed as [5]

$$\nu(t) = \nu_0(t) + \Delta\nu \cos(\omega t), \tag{1}$$

$$I(t) = I_0(t) + \Delta I \cos(\omega t + \Delta\varphi), \tag{2}$$

where ν_0 is the center frequency of the laser output, $\Delta\nu$ is the modulation frequency, ω is the modulation angular frequency, I_0 is the light intensity at the center frequency of the laser output, ΔI is the modulation amplitude of the light intensity, and $\Delta\varphi$ is the phase difference between the light intensity and the frequency.

In weak absorption conditions, according to the Taylor series expansion, the Beer–Lambert law can be expressed as

$$I_t(\nu) = I(\nu)[1 - \alpha(\nu)CL], \tag{3}$$

where I_t is the transmitted light intensity, C is the concentration of the gas to be measured, L is the length of the light-absorbing path, and $\alpha(\nu)$ is the absorption coefficient of the gas and is a periodic even function about ωt. $\alpha(\nu)$ can be expressed according to the Fourier series expansion as

$$\alpha(\nu) = \sum_{n=0}^{\infty} A_n \cdot \cos(n\omega t), \tag{4}$$

where A_n (n = 0, 1, 2, ...) is the Fourier expansion coefficient, which can be expressed as

$$\begin{array}{l} A_0 = \frac{1}{2\pi}\int_{-\pi}^{+\pi}[S(T)\varphi(\nu)P]\cdot d\theta \\ A_n = \frac{1}{\pi}\int_{-\pi}^{+\pi}[S(T)\varphi(\nu)P]\cdot \cos n\theta \cdot d\theta, n = 1,2,3\ldots \end{array} \quad (5)$$

where T is the temperature, $S(T)$ is the intensity of the absorption line at temperature T, P is the pressure, and $\varphi(\nu)$ is a line function.

Assuming that the circuit and optical path gain is ε and that the same frequency and phase reference signal given by the lock-in amplifier is $B\cos(2\omega t)$, then after demodulation, the second harmonic signal can be expressed as

$$X_{2f} = -\frac{1}{2}\varepsilon A_2 BCLI_0(t). \quad (6)$$

According to Equation (6), the measured gas concentration is proportional to the second harmonic value.

3. Variational Mode Decomposition

In 2014, Dragomiretskiy et al. proposed a non-recursive, completely adaptive signal decomposition method, which converts the signal decomposition problem into a variational problem by finding the optimal solution of the constrained variational problem model to achieve the adaptive decomposition of the signal [17], which decomposes the signal into the form of multiple intrinsic mode functions (IMFs) with finite bandwidth and different center frequencies. An IMF is defined as amplitude–frequency modulation (AM-FM) and is expressed as

$$\begin{array}{l} IMF(t) = A_k(t)\cos(\phi_k(t)) \\ \omega_k(t) = \phi_k{}'(t) \end{array} \quad (7)$$

where t is time; $\phi(t)$ is the phase, which is a non-decreasing function; $A_k(t)$ is the envelope amplitude of the IMF component, which is a non-negative number; $\omega_k(t)$ is the instantaneous frequency; and the instantaneous frequency and amplitude change at a slower rate than the phase. According to Carson's rule, the band of the IMF component can be expressed as

$$BW_{AM-FM} = 2(\Delta f + f_{FM} + f_{AM}), \quad (8)$$

where Δf is the maximum offset of the instantaneous frequency, f_{FM} is the instantaneous frequency offset rate, and f_{AM} is the highest frequency of the envelope $A_k(t)$.

The constrained variational problem model for solving the IMF component bandwidth can be expressed as [17]

$$\begin{array}{r} \min\limits_{\{IMF_k\},\{\omega_k\}}\left\{\sum\limits_k \left\|\partial_t\left[\left(\delta(t)+\frac{j}{\pi t}\right)*IMF_k(t)\right]e^{-j\omega_k t}\right\|_2^2\right\}, \\ s.t.\sum\limits_k IMF_k = X(t) \end{array} \quad (9)$$

where IMF_k and ω_k are the IMF components and their corresponding center frequencies, respectively; $X(t)$ is the original input signal; ∂_t is the partial derivative for t; δ_t is the impulse function; $*$ is the convolution sign; $\|\|_2$ is the norm of L; and *s.t.* represents the constraint. In order to obtain the constrained variational model of the IMF component bandwidth of Equation (8), a quadratic penalty factor (α) and a Lagrange multiplier operator (λ) are introduced, thus converting the constrained variational problem model into an unconstrained variational problem model. The quadratic penalty factor ensures the

accuracy of the reconstructed signal under noisy conditions, and the Lagrange multiplier operator ensures stricter constraints. They are brought into Equation (9) to obtain

$$\begin{aligned} L(\{IMF_k\},\{\omega_k\},\lambda) &= \alpha\sum_k \left\|\partial_t\left[(\delta(t)+\tfrac{j}{\pi t})*IMF_k(t)\right]e^{-jwt}\right\|_2^2 \\ &+\left\|X(t)-\sum_k IMF_k(t)\right\|_2^2+\left\langle\lambda(t),X(t)-\sum_k IMF_k(t)\right\rangle \end{aligned} \tag{10}$$

where $\langle,\rangle$ denotes the functional relationship between λ(t) and $X(t)-\sum_k IMF_k(t)$. The problem of finding the optimal solution of Equation (9) is transformed into the problem of finding the saddle point of Equation (10), and the saddle point can be solved using the cross-directional multiplier method.

4. Particle Swarm Optimization

Two parameters in the VMD-decomposed signal, the number of IMF components (K) and the penalty factor (α), have a strong influence on the decomposition results [18]. Therefore, the appropriate values of the two parameters become the core of the VMD algorithm, and the common method is to set the parameter values manually based on experience. Artificially finding the best values of the K and α parameters takes a lot of time, is not feasible, and ignores the influence between the two parameters. In order to find the values of the K and α parameters more quickly and reflect the performance of the VMD algorithm, an intelligent optimization algorithm can be used to find the two parameters. After comprehensive consideration, this paper used the particle swarm optimization algorithm to find the two parameters of K and α.

In 1995, the particle swarm optimization algorithm (PSO) was first proposed by Kennedy and Eberhart [19]. If there is a population of N particles in the target space and the population is updated by K iterations, then the i-th particle can be represented as the k-dimensional vector $X_i = (x_i^1, x_i^2, \ldots, x_i^k)$, $i = 1,2, \ldots L$; the velocity of the i-th particle is $V_i = (v_i^1, v_i^2, \ldots, v_i^k)$, $i = 1,2, \ldots L$; the i-th particle so far in the search for the individual optimal solution is $P_{\text{best}} = (p_i^1, p_i^2, \ldots, p_i^k)$, $i = 1,2, \ldots$ L; and the global optimal solution searched by the whole particle swarm so far is $g_{\text{best}} = (p_g^1, p_g^2, \ldots, p_i^k)$, $i = 1,2, \ldots$ L. When the individual optimal solution and the global optimal solution are found, the particle updates the individual's position and velocity according to Equations (11) and (12):

$$x_i^{k+1} = x_i^k + v_i^k, \tag{11}$$

$$v_i^{k+1} = w \times v_i^k + c_1 r_1 (p_i^k - x_i^k) + c_2 r_2 (p_g^k - x_i^k), \tag{12}$$

where c_1 and c_2 are learning factors; r_1 and r_2 are random numbers in the range [0, 1]; $\omega \times v_i^k$ is the particle's own inertia, indicating that the particle keeps its own velocity; $c_1 r_1 (p_i^k - x_i^k)$ is the tendency to learn from its own experience and make approximations to its own historical optimum; and $c_2 r_2 (p_g^k - x_g^k)$ is the tendency of the particle to learn the historical optimum in the population and to make an approximation to the optimal position of the population. The transformation of the particle in the solution space is shown in Figure 1.

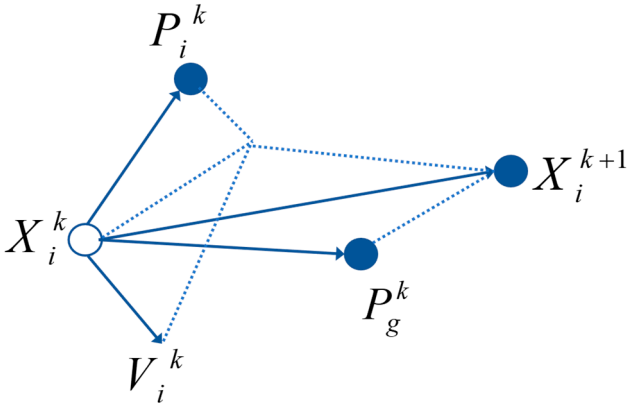

Figure 1. The way the particles transform in the solution space.

The fitness function in the particle swarm optimization algorithm is a qualification of the optimization parameters, and in this paper we chose the envelope entropy value of the last IMF component as the fitness function. The smaller the envelope entropy, which indicates the single frequency component, the more concentrated the instantaneous envelope value of the signal and the better the signal. The envelope entropy can be expressed as

$$p_i = \frac{A(t)}{\sum_{t=1}^{N} A(t)}, \tag{13}$$

$$E = -\sum_{i=1}^{N} p_i * \log p_i. \tag{14}$$

where $A(t)$ is the envelope signal of the last IMF, which contains components altered by the Hilbert transform; p_j is the normalized form of the envelope signal, $A(t)$, of the last IMF component; N is the length of the last IMF component; and i is the i-th point of the last IMF component sequence.

5. Signal Reconstruction

Through the PSO algorithm's iterative optimization search, it is necessary to select the appropriate IMF components for the reconstructed signal after noise reduction. In this paper, the correlation coefficient, standard signal, and correlation coefficient threshold are introduced to complete the reconstructed signal.

The correlation coefficient [20] is a common statistical indicator in statistics and is used to study the degree of linear correlation between two variables. The VMD decomposition of K and α is calculated based on the results of the fitness function and decomposed into K IMF components. The correlation coefficient of each IMF component with the standard signal is calculated separately. Coefficients of correlation are used to distinguish whether each IMF component prefers the signal or the noise. A larger correlation coefficient indicates that the IMF prefers the signal, and the correlation coefficient can be expressed as

$$R = \frac{E[IMF_k(t)X(t)] - E[IMF_k(t)]E[X(t)]}{\sqrt{D[IMF_k(t)]}\sqrt{D[X(t)]}}. \tag{15}$$

where $X(t)$ is the standard signal, $IMF_k(t)$ is the IMF component after VMD decomposition, E is the mathematical expectation, and D is the mathematical variance. The standard signal is a noise-free simulated second harmonic signal of 100 ppm. The correlation coefficient threshold was chosen as 1/10 of the maximum correlation coefficient.

The PSO-VMD algorithm performs the noise reduction steps on the signal as follows:

1. Initialize the PSO and VMD parameters and set the envelope entropy as the fitness function;

2. Given the randomly generated particle position (that is, random K and α) and the finding range of the particle, determine the initial velocity of the particle;
3. According to the different particle positions, calculate the value of the adaptation function corresponding to the VMD decomposition (that is, the envelope entropy value of the last IMF component);
4. Comparing the different fitness function values, the smallest fitness function value is used to update the individual optimal value and the global optimal value and to update the velocity and position of the particle;
5. Repeat steps (3) to (5) until the given number of iterations is reached and the optimal solution of the particle is output;
6. According to the optimal solution (K and α) obtained in step (5), use VMD to decompose, obtain K IMF components, and calculate each IMF component with the standard signal correlation coefficient;
7. According to the given threshold value of the correlation coefficient, choose the IMF components to reconstruct the signal and add the selected IMF components to obtain the restructured signal after the noise is reduced.

A flow chart of the PSO-VMD algorithm for signal noise reduction is shown in Figure 2.

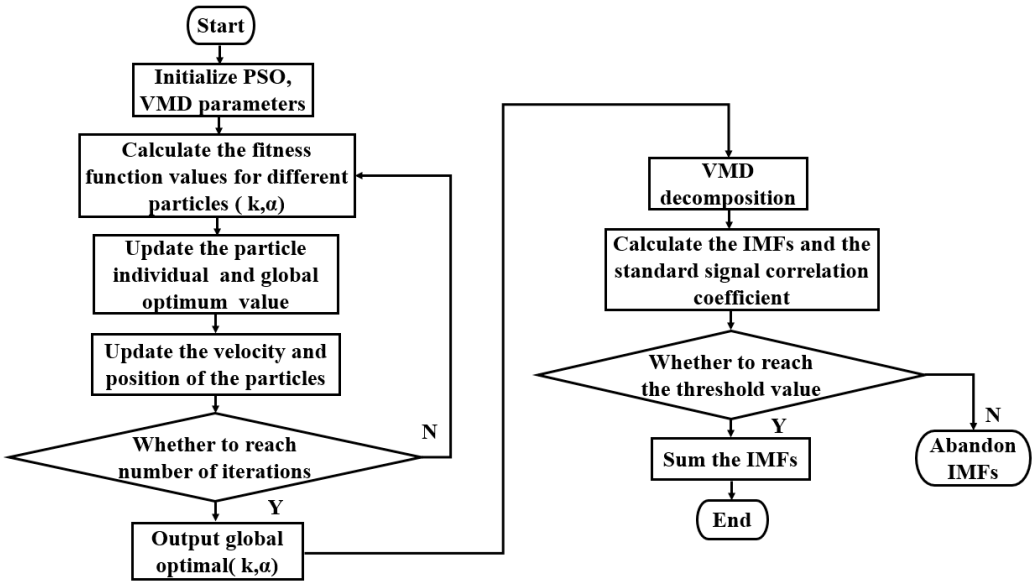

Figure 2. Flow chart of PSO-VMD algorithm for signal noise reduction.

6. Simulation Results and Analysis

In this paper, MATLAB software was used to write a program to simulate the second harmonic signal. The CH_4 absorption spectral line at 6046.96 cm^{-1} was used for the simulation, and the data about the CH_4 absorption spectral line at 296 K were obtained from the HITRAN database, as shown in Table 1.

Table 1. Spectroscopic parameters of the selected CH_4 transition near 6046.96 cm^{-1} (296 K).

ν (cm^{-1})	S (cm^{-1}/(molecule·cm^{-2}))	γ_{air} (cm^{-1} atm^{-1})	γ_{self} (cm^{-1} atm^{-1})	E′′ (cm^{-1})
6046.943	7.877×10^{-22}	0.0651	0.079	62.8758
6046.952	9.277×10^{-22}	0.0774	0.079	62.8768
6046.964	1.455×10^{-21}	0.0578	0.079	62.8782

ν is the wave number, S is the absorption line intensity, γ_{air} is the air-broadening coefficient, γ_{self} is the self-broadening coefficient, and E′′ is the energy at the lower level.

6.1. Threshold of Correlation Coefficient

There are no specific criteria for the value of the correlation coefficient with the degree of correlation, and the selection of the correlation coefficient threshold value affects the number of IMFs in the reconstructed signal and the accuracy of the reconstructed signal with noise reduction. In order to find the correlation coefficient threshold value, the noisy second harmonic signals of the 200 ppm and 1000 ppm concentrations were selected for PSO-VMD, processed, and discussed. The correlation coefficient threshold values were set to 0.5, 1/2 of the maximum correlation coefficient, and 1/10 of the maximum correlation coefficient, and the IMFs that satisfied the correlation coefficient threshold conditions were added in all three cases to obtain the reconstructed second harmonic signals. In TDLAS gas detection systems, the maximum value of the second harmonic signal is usually used to invert the concentration of the gas. Therefore, the residual of the reconstructed second harmonic signal with the peak value of the non-noisy second harmonic signal was calculated under different correlation coefficient threshold conditions, as shown in Table 2.

Table 2. Residuals of the maximum value of the reconstructed signal and the noiseless second harmonic signal under different correlation coefficient thresholds.

Concentration (ppm)	0.5	1/2 of the Maximum Correlation Coefficient	1/10 of the Maximum Correlation Coefficient
200	4.17×10^{-3}	4.17×10^{-3}	-5.92917×10^{-4}
1000	1.793×10^{-2}	-2.76×10^{-3}	-8.1379×10^{-5}

From Table 2, it can be seen that the second harmonic peak recovery was best when the correlation coefficient threshold value was 1/10 of the maximum value in the correlation coefficient.

At conditions of 296 K, 1 atm, and a 300 cm optical absorption path, the second harmonic signal of CH_4 gas was simulated with a trapezoidal wave as the scanning signal and a sine wave as the modulation signal at concentrations from 100 ppm to 1000 ppm, and random noise, including white noise and interference noise, was added at different concentrations.

The parameters in the PSO-VMD algorithm were set as follows: the range of K was 3–20, the range of α was 2000–5000, the number of iterations was 60, the number of particles was 30, the learning factors were $c_1 = 2$ and $c_2 = 2$, the maximum value of the particle velocity was 1, the minimum value was -1, and the inertia weight was 0.5. In order to show the effectiveness and feasibility of the PSO-VMD algorithm, the filtering performances of wavelet filtering, SG filtering, and the PSO-VMD algorithm were compared in terms of SNR and linearity. After continuous sampling, the wavelet filtering algorithm with the best filtering effect was finally selected with the wavelet basis function "db4", and the number of decomposition layers was 7. The polynomial of SG filtering had a fitting order of 3 and a window length of 5.

6.2. SNR Comparison

The three methods of wavelet filtering, SG filtering, and PSO-VMD were used to denoise the second harmonic signals of 10 sets of concentrations. Taking the second harmonic signal with the 500 ppm concentration as an example, the three algorithms of SG filtering, wavelet filtering, and PSO-VMD were used to process the second harmonic signal with noise, as shown in Figure 3.

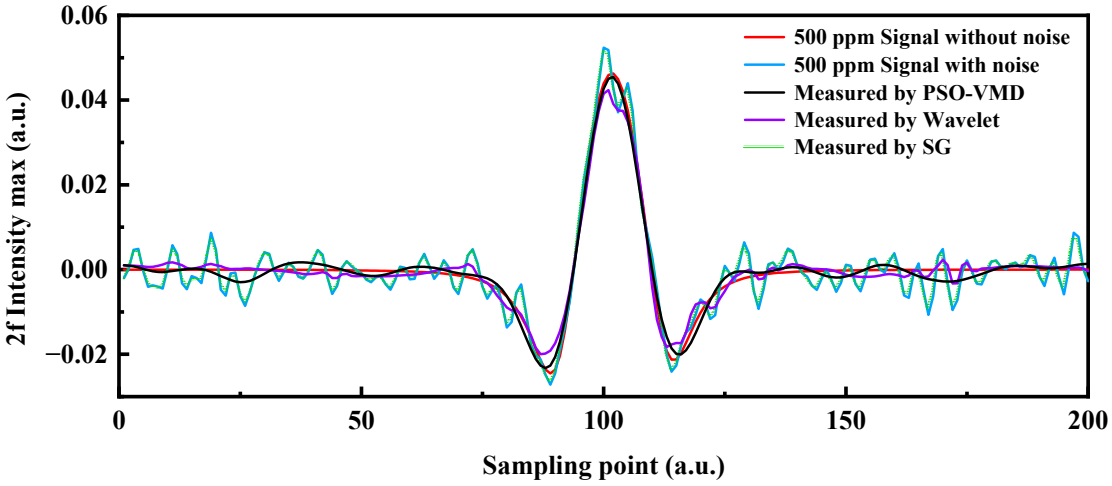

Figure 3. Noise reduction of three methods on second harmonic signals at 500 ppm.

It can be seen from Figure 3 that the SG denoising effect was not significantly improved. Wavelet filtering had the maximum offset phenomenon, and PSO-VMD had the best result, where the second harmonic signal was basically coincident with the pure second harmonic signal after the denoising, which could indicate that the PSO-VMD algorithm has a good denoising effect. In order to reflect the recovery effects of different algorithms on the second harmonic peaks more intuitively, the residuals between the maximum values of the noisy second harmonic signal, the wavelet-denoised signal, the SG-denoised signal, the PSO-VMD-denoised signal, and the maximum value of pure second harmonic signal were calculated as 0.00608, −0.00393, 0.0533, and −0.00082, respectively. Considering the fluctuation of the two wings of the second harmonic and the overall fluctuation of the noise, the residuals between the standard deviations of the noisy second harmonic signal, wavelet-denoised signal, SG-denoised signal, and PSO-VMD-denoised signal and the standard deviation of the pure second harmonic signal were calculated as 0.01186, 0.01175, 0.00995, and 0.01069, respectively. Considering the second harmonic peak recovery, the noise fluctuation of both wings, and the overall noise reduction, it can be seen that the PSO-VMD algorithm had a good noise reduction effect.

The SNR enhancement effects of the three methods of wavelet filtering, SG filtering, and PSO-VMD on 10 sets of noisy second harmonic signals of different concentrations are shown in Table 3.

Table 3. SNR values of three algorithms for noise signals of different concentrations.

Concentration (ppm)	Original Signal (dB)	PSO-VMD (dB)	SG (dB)	Wavelet (dB)
100	−2.38962	1.64915	−1.89101	1.52418
200	0.65962	4.07643	1.11542	3.69764
300	2.81747	5.79828	3.20817	5.01898
400	3.59861	6.70118	3.9552	5.80353
500	4.83354	8.57604	5.32585	7.75379
600	5.60625	7.75962	6.02992	7.18978
700	6.08892	8.51311	6.53482	8.01657
800	6.45367	8.66172	6.99472	6.60428
900	6.52896	8.57667	6.89811	7.86203
1000	7.00384	9.33913	7.39223	9.17129

From Table 3, it can be seen that in different concentrations of noisy second harmonic signals, the PSO-VMD adaptive algorithm had the best SNR improvement compared with SG and wavelet filtering. At low concentrations, the SNR was improved by 4.03877 dB compared to the noisy second harmonic signal. At high concentrations of 800 ppm and

900 ppm, the SG and wavelet filtering showed fluctuations in the SNR, but the PSO-VMD algorithm was still stable.

6.3. Linearity Comparison

Linearity can be a measurement of the stability of a system, as can the offset of each concentration point and the degree of linearity of the predicted values. The maximum value of the second harmonic in harmonic detection can reflect the gas concentration, so the maximum values of the noisy second harmonic signal, wavelet-denoised signal, SG-denoised signal, and PSO-VMD-denoised signal were linearly fitted to the corresponding gas concentrations, and the results are shown in Figure 4.

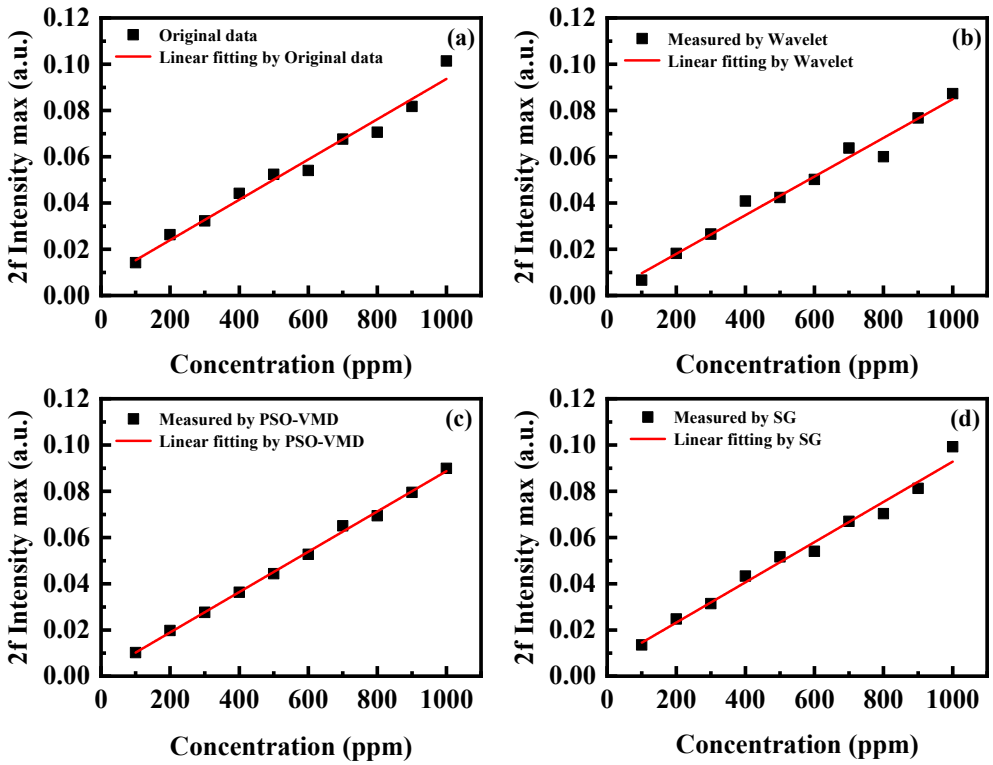

Figure 4. Linear analysis of noisy signal and noise reduction using three methods. (**a**) The linear fitting relationship between the second harmonic maximum and the concentration of the original data; (**b**) The linear fitting relationship between the second harmonic maximum and the concentration processed by wavelet transform; (**c**) The linear fitting relationship between the second harmonic maximum and the concentration processed by PSO-VMD; (**d**) The linear fitting relationship between the second harmonic maximum and the concentration processed by SG.

Figure 4 corresponds to the linear fitting relationship equation and the correlation coefficient (R^2), as shown in Table 4.

Table 4. Linear fitting and R^2 values of three methods.

Signal	Linear Fitting	R^2
Original signal	$y = 8.71042 \times 10^{-5}x + 0.00655$	0.97743
Wavelet	$y = 8.3589 \times 10^{-5}x + 0.00129$	0.97698
PSO-VMD	$y = 8.71866 \times 10^{-5}x + 0.00151$	0.99782
SG	$y = 8.69668 \times 10^{-5}x + 0.00581$	0.98296

From Table 4, it can be seen that the correlation coefficient (R^2) was improved from 0.97743 to 0.99798 after noise reduction by the PSO-VMD algorithm, which had the highest linearity compared to the other methods. The intercept of the linear fitting equation

represents the original background noise, which was reduced from 0.00665 to 0.00151 after the processing of the noisy signal by the PSO-VMD algorithm, which also indicated a further reduction in noise. In addition, the linearity of the original data processed by the PSO-VMD and SG algorithms showed a similar relationship due to the influence of the background noise, while the linearity of the wavelet transform was slightly different because the peak of the second harmonic was shifted after the algorithm was processed.

7. Experimental Results and Analysis

In the experiment, methane was used as the target gas to be measured, and the absorption spectrum of 1653.7 nm was selected. The laser was a DFB laser with its output centered around 1653 nm, and an LDC501 laser controller was used to drive the DFB laser, which scanned the center wavelength of the absorption spectrum. The modulation signal of the laser was generated by two signal generators that separately produced a 4 kHz sine wave signal and a 0.9 Hz trapezoidal wave signal. Using an RCS2000 automatic gas distribution system, 10,000 ppm methane and high-purity nitrogen were mixed and configured into different concentrations of methane gas, and the gas was injected into the gas absorption cell. The PD photodetector, made of InGaAs, received the transmitted beam and converted the light signal into a current signal, which was further converted into a voltage signal by a transimpedance amplifier. Then, the signal was transmitted to a lock-in amplifier for demodulation. The reference signal of the lock-in amplifier was a sine wave of 8 kHz that was generated synchronously by the signal generator generating the 4 kHz sine wave signal, and finally the second harmonic signal was gathered by a computer and filtered. A structure diagram of the TDLAS system is shown in Figure 5.

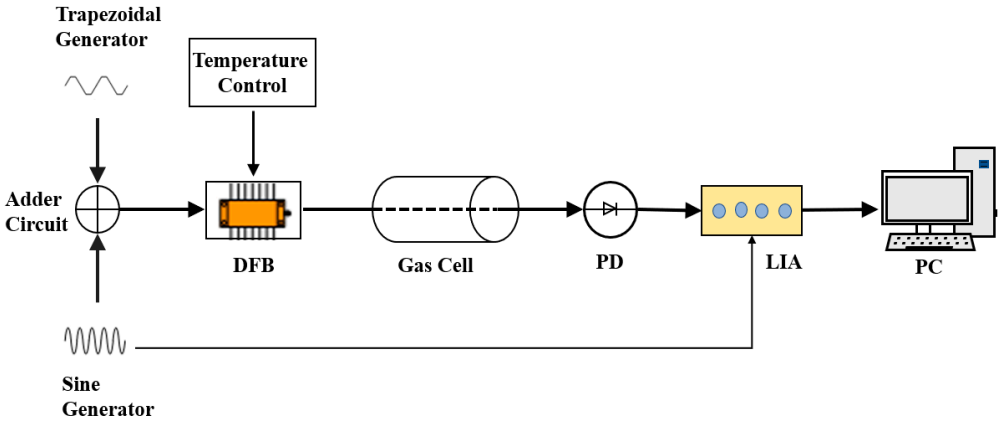

Figure 5. TDLAS experimental setup.

The same parameters were set as in the simulation analysis. PSO-VMD was used to process the experimental second harmonic signal for the concentration range of 200–1000 ppm.

7.1. Linearity Analysis

A linear fitting between the experimental concentrations and their corresponding second harmonic maximums was obtained, as shown in Figure 6.

The linear relationship was fitted to a line with $\max(2f) = 7.59569 \times 10^{-5}\ C + 0.00994$ and a correlation coefficient of $R^2 = 0.99733$. The good denoising performance and the stability of the peak recovery of the PSO-VMD algorithm were proven.

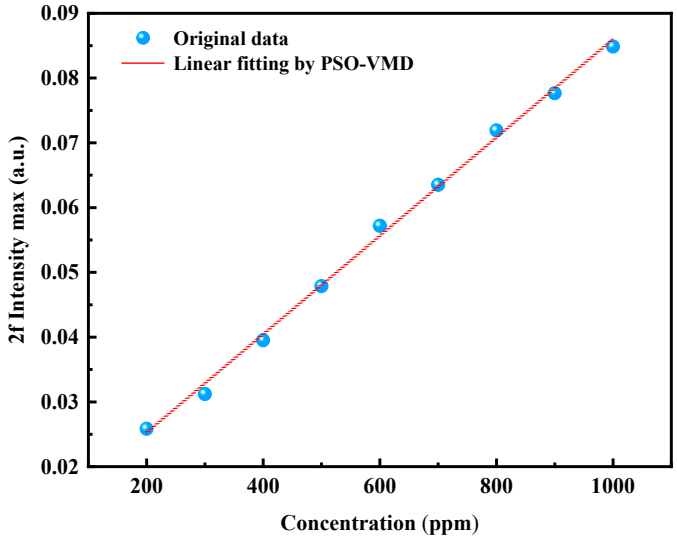

Figure 6. Linear fitting of concentrations and second harmonic signal maximums processed by PSO-VMD.

7.2. Stability Evaluation

In order to verify the stability of the PSO-VMD algorithm, the second harmonic signals of gases with 500 ppm concentrations were collected continuously over several hundred cycles. The second harmonic signal maximum processed by the PSO-VMD algorithm and the original experimental signal were analyzed separately, and the concentration was inverted by the linear relationship between the respective concentration and the second harmonic maximum. The original data, processed by the PSO-VMD algorithm for the stability of the concentration, and their correlation with a Gaussian distribution are shown in Figure 7.

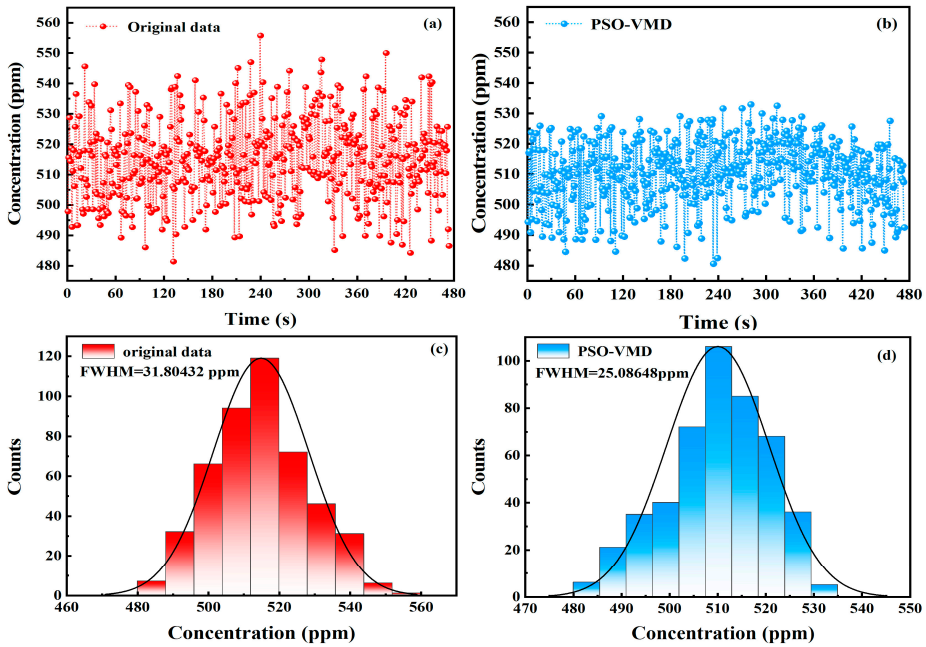

Figure 7. Multiple 500 ppm cycles of concentration inversion. (**a**) Original data of 500 ppm stability; (**b**) Stability of 500 ppm after PSO-VMD processed; (**c**) Gaussian distribution of original data 500 ppm; (**d**) Gaussian distribution of 500 ppm by PSO-VMD processed.

The standard deviation and mean values of the original experimental data and the data processed by the PSO-VMD algorithm are shown in Table 5.

Table 5. Standard deviation (SD) and mean values of original data and data processed by PSO-VMD.

Signal	SD (ppm)	Average (ppm)
Original signal	13.50605	514.83586
PSO-VMD	10.65325	510.02011

It can be seen that after the PSO-VMD algorithm processing, the prediction accuracy and stability were significantly improved, with a good Gaussian distribution characteristic. In addition, the mean value of the original signal was raised due to the background interference introduced by the modulated signal compared with the PSO-VMD algorithm. The background noise was effectively reduced by 4.82 ppm, and the standard deviation was also reduced, which also proved that the PSO-VMD algorithm improved the stability and detection accuracy of the TDLAS system.

8. Conclusions

In this paper, a PSO-VMD adaptive algorithm was proposed. Using the same standard, which was the same standard signal and correlation coefficient threshold, we achieved the suppression of noise in both simulated and experimental second harmonic signals, which reflected the adaptiveness of the algorithm in TDLAS. For the simulated data, we compared the noise reduction results of SG filtering, wavelet filtering, and PSO-VMD in two aspects: linearity and SNR. The SNR improvement results were the best, and the linear fitting correlation coefficient was also the highest. The SNR could be improved by 4.03877 dB, and the correlation coefficient (R^2) of linearity was improved from 0.97743 to 0.99798. For the experimental data, a good linear fit was obtained after PSO-VMD processing, with a correlation coefficient of $R^2 = 0.99733$, and the background noise interference was effectively reduced, which improved the stability and detection accuracy of the TDLAS system. In conclusion, the PSO-VMD adaptive algorithm provides a new method for TDLAS signal noise reduction and has good results compared with SG and wavelet filtering.

Author Contributions: Conceptualization, M.M. and J.C.; methodology, M.M. and J.S.; software, M.M. and J.C.; data curation, M.M. and S.L.; formal analysis, M.M. and Z.W.; investigation, J.C.; writing—original draft preparation, M.M.; writing—review and editing, M.M. and J.C. All authors have read and agreed to the published version of the manuscript.

Funding: This research received no external funding.

Institutional Review Board Statement: Not applicable.

Informed Consent Statement: Not applicable.

Data Availability Statement: The data presented in this study are available from corresponding authors.

Conflicts of Interest: The authors declare no conflict of interest.

References

1. Henderson, B.; Khodabakhsh, A.; Metsälä, M.; Ventrillard, I.; Schmidt, F.M.; Romanini, D.; Ritchie, G.A.D.; Hekkert, S.T.L.; Briot, R.; Risby, T.; et al. Laser spectroscopy for breath analysis: Towards clinical implementation. *Appl. Phys. B* **2018**, *124*, 161. [CrossRef] [PubMed]
2. Jin, Z.; Jorns, A.; Yim, W.; Wing, R.; Mantri, Y.; Zhou, J.; Zhou, J.; Wu, Z.; Moore, C.; Penny, W.F.; et al. Mapping Aerosolized Saliva on Face Coverings for Biosensing Applications. *Anal. Chem.* **2021**, *93*, 11025–11032. [CrossRef] [PubMed]
3. Nguyen, P.Q.; Soenksen, L.R.; Donghia, N.M.; Angenent-Mari, N.M.; de Puig, H.; Huang, A.; Lee, R.; Slomovic, S.; Galbersanini, T.; Lansberry, G.; et al. Wearable materials with embedded synthetic biology sensors for biomolecule detection. *Nat. Biotechnol.* **2021**, *39*, 1366–1374. [CrossRef] [PubMed]
4. Li, J.; Yu, B.; Zhao, W.; Chen, W. A Review of Signal Enhancement and Noise Reduction Techniques for Tunable Diode Laser Absorption Spectroscopy. *Appl. Spectrosc. Rev.* **2014**, *49*, 666–691. [CrossRef]
5. Sun, J.; Chang, J.; Wei, Y.; Lin, S.; Wang, Z.; Mao, M.; Wang, F.; Zhang, Q. Feature Domain Transform Filter for the Removal of Inherent Noise Bound to the Absorption Signal. *Anal. Chem.* **2022**, *94*, 14290–14298. [CrossRef] [PubMed]

6. Kireev, S.V.; Kondrashov, A.A.; Shnyrev, S.L. Application of the Wiener filtering algorithm for processing the signal obtained by the TDLAS method using the synchronous detection technique for the measurement problem of $^{13}CO_2$ concentration in exhaled air. *Laser Phys. Lett.* **2019**, *16*, 085701. [CrossRef]
7. Luo, Q.; Yang, C.; Song, C.; Zhou, J.; Gui, W. TDLAS/WMS Embedded System for Oxygen Concentration Detection of Glass Vials with Variational Mode Decomposition—ScienceDirect. *IFAC-PapersOnLine* **2020**, *53*, 11626–11631. [CrossRef]
8. Li, J.; Deng, H.; Li, P.; Yu, B. Real-time infrared gas detection based on an adaptive Savitzky-Golay algorithm. *Appl. Phys. B-Lasers Opt.* **2015**, *120*, 207–216. [CrossRef]
9. Luo, Q.; Zhou, J.; Li, W.; Yang, C.; Gui, W. Interference Fringe Suppression for Oxygen Concentration Measurement Using Adaptive Harmonic Feeding Generative Adversarial Network. *IEEE Sens. J.* **2022**, *22*, 2419–2429. [CrossRef]
10. Tang, Q.X.; Gao, H.; Zhang, Y.J.; Chen, D. Elimination of Scintillation Noise Caused by External Environment Disturbances in Open Space. *Photonics* **2022**, *9*, 415. [CrossRef]
11. Wang, S.; Gong, W.; Wang, Z.; Wei, Y.; Li, Y.; Zhang, T.; Zhang, Q.; Zhang, L.; Song, F.; Zhang, W.; et al. Interference fringe suppression in tunable diode laser absorption spectroscopy based on CEEMDAN-WTD. *Front. Phys.* **2022**, *10*, 1109. [CrossRef]
12. Hou, G.; Xu, L.; Zhou, W.; Huang, A.; Cao, Z. A Interferometer modulated TDLAS Temperature Sensor by using Coherent Demodulation. In Proceedings of the IEEE International Instrumentation and Measurement Technology Conference (I2MTC), Ottawa, ON, Canada, 16–19 May 2022.
13. Luo, Q.; Song, C.; Yang, C.; Gui, W.; Sun, Y.; Jeffrey, Z. Headspace Oxygen Concentration Measurement for Pharmaceutical Glass Bottles in Open-Path Optical Environment Using TDLAS/WMS. *IEEE Trans. Instrum. Meas.* **2020**, *69*, 5828–5842. [CrossRef]
14. Meng, Y.; Liu, T.; Liu, K.; Jiang, J.; Wang, R.; Wang, T.; Hu, H. A Modified Empirical Mode Decomposition Algorithm in TDLAS for Gas Detection. *IEEE Photonics J.* **2014**, *6*, 1–7. [CrossRef]
15. Chen, H.; Liu, S. TDLAS Signal Denoising with the EEMD and Monkey King Evaluation Method. In Proceedings of the 2019 IEEE 4th International Conference on Image, Vision and Computing (ICIVC), Xiamen, China, 5–7 July 2019.
16. Dragomiretskiy, K.; Zosso, D. Variational Mode Decomposition. *IEEE Trans. Signal Process.* **2014**, *62*, 531–544. [CrossRef]
17. Liu, Y.; Yang, G.; Li, M.; Yin, H. Variational Mode Decomposition Denoising Combined the Detrended Fluctuation Analysis. *Signal Process.* **2016**, *125*, 349–364. [CrossRef]
18. Luo, D.; Zhang, M.; Wang, Z. A Low-Noise Chopper Amplifier Designed for Multi-Channel Neural Signal Acquisition. *IEEE J. Solid-State Circuits* **2019**, *54*, 2255–2265. [CrossRef]
19. Kennedy, J.; Eberhart, R. Particle swarm optimization. In Proceedings of the 1995 IEEE International Conference on Neural Networks Proceedings (Cat. No.95CH35828), Perth, Australia, 27 November–1 December 1995.
20. Yan, H.; Xu, T.; Wang, P.; Zhang, L.; Hu, H.; Bai, Y. MEMS Hydrophone Signal Denoising and Baseline Drift Removal Algorithm Based on Parameter-Optimized Variational Mode Decomposition and Correlation Coefficient. *Sensors* **2019**, *19*, 4622. [CrossRef] [PubMed]